JEE Journal of Ecological Engineering

Journal of Ecological Engineering, 2026, 27(9), 196–215
https://doi.org/10.12911/22998993/221601
ISSN 2299–8993, License CC-BY 4.0

Received: 2026.04.10
Accepted: 2026.07.15
Published: 2026.08.01

Optimizing production parameters for enhanced properties of licorice root residue-based activated carbons

Shahrom Khoshimov[1], Mirtokhir Muratov[1*], Nilufar Rahmonaliyeva[1], Aziza Abdikamalova[4], Izzat Eshmetov[1], Shakhnoza Kuldasheva[2], Nozim Mamataliev[1], Nursultan Maratov[1], Rasulbek Eshmetov[3], Oksana Seitnazarova[4]

[1] Institute of General and Inorganic Chemistry, Academy of Sciences of the Republic of Uzbekistan, Tashkent 100170, Uzbekistan
[2] Termiz State Pedagogical Institute, Termiz, Uzbekistan
[3] Mamun University, Khiva, Xorazm Region, Uzbekistan
[4] Karakalpak State University, 1 Gulbadam Street, Nukus 742012, Karakalpakstan, Uzbekistan
* Corresponding author's e-mail: muratovmirtoxir@mail.ru

ABSTRACT

This study explores how production conditions affect the properties of activated carbons derived from licorice root residue, focusing on their textural and adsorptive characteristics. Key parameters, including carbonization temperature and KOH concentration during activation, were varied to assess their impact on pore structure, surface area, pore volume, and adsorption capacity. Results showed that both temperature and KOH concentration significantly influenced porosity and adsorption performance. Thermochemical activation produced carbon with a pore volume ten times greater than that from thermal activation alone. Chemical activation using KOH enhanced surface area and pore structure, with the AC5-800 sample exhibiting a surface area of 917.69 m^2/g and micropore and mesopore volumes of 0.487 cm^3/g and 0.5167 cm^3/g, respectively. The optimal biocarbon-to-KOH ratio for porosity was 1:5, balancing adsorption of large and small molecules. Ratios of 1:3 and 1:7 reduced pore volume, with overactivation damaging smaller pores at 1:7. AC5-800 exhibited the highest MB uptake, attributed to its specific surface area of 31.42 m^2/g and pore volume of 0.0497 cm^3/g. Adsorption data fitted well to the Langmuir isotherm ($R^2 = 0.995$), indicating that the adsorption mechanism followed monolayer coverage on a homogeneous surface These findings highlight licorice root residue as a sustainable, cost-effective raw material for activated carbon production, with potential applications in aquatic pollutants. The study underscores its promise as an effective adsorbent for environmental protection.

Keywords: adsorption, biomass-derived carbons, environmental remediation, waste valorization.

INTRODUCTION

Activated carbon plays a critical role in industrial applications, with annual demand exceeding 1 million tons and projected growth rates of 9–10% per year. However, more than 85% of its production relies on non-renewable resources such as carbon and petroleum products, necessitating the exploration of alternative sources. Plant residues, such as tree bark and agricultural waste, offer a sustainable solution, providing both environmental benefits and effective waste utilization. The production of activated carbon is influenced by parameters such as temperature, activation agent concentration, and carbonization time, which affect key properties like surface area, porosity, and adsorption capacity. The structure of activated carbon makes it suitable for pollutant adsorption, and it is extensively used in industries for water purification and air treatment (Ghorbani et al., 2020; Wan Ibrahim et al., 2019; Shafeeyan et al., 2010; Choi and Lee, 2015).

In light of increasing environmental concerns, plant-based activated carbon presents an effective solution for water purification (De Gisi et al., 2016). It facilitates waste management, while

aligning with the UN Sustainable Development Goals (Liu and Zhang, 2022). This work focuses on optimizing production parameters to enhance the efficiency of activated carbons derived from agricultural residues such as licorice root, aiming to minimize environmental impact, while improving adsorption properties (Dawood, 2018).

Utilizing licorice root residue helps control agricultural waste, which otherwise poses disposal challenges and environmental hazards. By converting this waste into valuable activated carbon, the process not only reduces the environmental footprint, but also supports sustainable waste management practices. This aligns with the principles of circular economy, turning waste into a resource (Garg et al., 2023). This approach also supports global sustainability goals by providing an eco-friendly method for producing activated carbon. It also addresses waste minimization, resource recovery, and pollution reduction, contributing to the development of greener technologies.

In recent years, the global demand for activated carbons in water purification, and other industrial applications continues to grow. Developing activated carbon from licorice root residue provides a cost-effective option to conventional sources like carbon and wood, making it attractive for large-scale industrial use. This would add economic value to agricultural by-products and can stimulate local economies where it is cultivated.

This study seeks to optimize the production process, aiming to enhance resource utilization and reduce the environmental footprint associated with activated carbon production (Sen, 2017). Enhancing the properties of activated carbon improves their adsorption capacity, making it more efficient in applications such as water purification and pollutant removal in industrial settings. Optimizing production parameters can also result in cost-effective methods for producing high-quality activated carbons, benefiting industries that depend on these materials (Qu et al., 2019).

For commercial viability, an ideal adsorbent needs to possess essential characteristics, including a substantial internal surface area, high affinity for specific compounds, easy regenerability, resistance to degradation, and stability in diverse environments (Sen, 2023). Various materials with high porous structures, both carbonaceous and inorganic, can serve as effective adsorbents. Their effectiveness depends on its surface area and chemical composition, with its internal pores contributing to its voluminous structure (Blachnio et al., 2020).

Carbon adsorbents produced from waste and secondary materials demonstrate high efficiency in pollutant removal, achieving purification levels between 80 and 99%, making them essential for sustainable water resource management strategies (Zhang et al., 2017). However, while various technologies exist for producing carbon adsorbents, not all are universally applicable. Many production methods require significant raw material and energy inputs, making them energy- and labor-intensive (Rizkiana et al., 2014). Therefore, refining production methods for carbon adsorbents from waste and low-value materials remains crucial. Thermochemical activation using chemical agents such as KOH, K_2CO_3, NaOH, and $ZnCl_2$ can enhance the porous structure of carbon adsorbents by reducing ash content in plant materials and promoting pore development (Muttil et al., 2022).

In recent years, interest in using plant residues for carbon adsorbent production has increased due to their environmental and economic benefits. Plant residues provide readily available and renewable sources of raw materials. Licorice root residue shows promise due to its abundance in Uzbekistan, where licorice is extensively cultivated and processed. Converting licorice root residue into carbon adsorbents offers potential for environmental remediation and waste utilization (Tibor and Grande, 2022). The conversion of licorice root residue into activated carbon is justified by its inherent chemical properties, environmental and economic advantages, and the potential to enhance specific adsorptive characteristics through controlled processing conditions. This makes it a promising candidate for sustainable and efficient pollutant removal solutions.

Previous studies might have underestimated licorice root residue as a viable feedstock for activated carbon production. They have not thoroughly optimized production parameters, such as carbonization temperature, activation methods, or chemical activator concentrations for licorice root residue-derived carbons (Soffian et al., 2022). Additionally, prior research might have lacked detailed characterization of the resulting activated carbons, including specific surface area, pore volume, and adsorption capacity (Yahya et al., 2015), and often focus on synthesis without addressing practical applications (Wang et al., 2023). Despite extensive research on plant residues, there is a gap in exploring the chemical activation of licorice root residues and the development of porous

structures in adsorbents derived from this material. Therefore, further investigation into activation processes and the formation of porous structures in licorice root residue-derived adsorbents is needed (El Qada et al., 2008).

To address existing knowledge gaps, this study aims to repurpose licorice root residue into high-value activated carbon, tackling the issues of waste management and resource inefficiency at the same time. This work determines optimal conditions for the thermal and chemical activation of carbonization using licorice root residues and investigates the mechanisms of porous structure formation under various activation methods. Several characterization techniques were employed to analyze the porous structures of the activated carbons and correlate their properties with production parameters. Additionally, the study assesses the suitability of the activated carbons for wastewater treatment and optimizes production parameters to enhance material properties, ensuring that the activated carbons meet the specific requirements of different applications.

This study explores the production of adsorbent materials from licorice root, an industrial waste byproduct, for the removal of various harmful substances from wastewater. By leveraging the high carbon content and potential porosity of this waste material post-activation, the research offers a sustainable method to valorize waste while mitigating environmental impacts. The investigation focuses on optimizing production parameters such as carbonization temperature, activation methods, and activating agent concentrations to enhance key properties like surface area, pore volume, and adsorption capacity. These tailored activated carbons are designed for diverse applications, including water treatment, air purification, and pollutant removal (Ali et al., 2012).

The work underscores the importance of sustainable production practices by repurposing agricultural waste and optimizing resource efficiency. It aligns with the growing emphasis on sustainability in materials science and engineering, advancing efforts in environmental sustainability and innovation in material science (Usmanov et al., 2020). By fine-tuning carbonization and activation conditions, such as temperature and chemical agents, the study anticipates significant improvements in the surface area and pore volume of the activated carbons. This enhancement is expected to yield highly efficient adsorbents capable of removing pollutants like dyes and volatile organic compounds effectively.

MATERIALS AND METHODS

Materials

Residual biomass, specifically licorice root residues (LRR), was utilized as the raw material. The residues were washed with deionized water to remove surface impurities, oven-dried at 105 °C for 24 hours, and subsequently ground into fine powder using a laboratory mill (Retsch SM 200). The powder was sieved to obtain particles with a diameter below 500 μm for uniform processing.

Carbonization process

The dried licorice root powder was subjected to isothermal carbonization within a horizontal tubular furnace (Carbolite Gero STF 15). To maintain a strictly inert atmosphere and prevent oxidation, the furnace was purged with high-purity nitrogen (N_2, 99.99%) at a constant flow rate of 50 mL/min. For each experimental run, a sample mass of 5.0 $\pm$ 0.1 g was weighed and placed in a high-purity alumina crucible (50 mL capacity) (Askarova et al., 2025).

The furnace was heated at a linear rate of 10 °C/min until reaching the target carbonization temperature. The samples were processed across a temperature range of 500–900 °C with residence times varying between 60 and 300 min. Following the dwell period, the furnace was allowed to cool naturally to ambient temperature under a continuous N_2 flow to protect the carbon matrix. The resulting carbonized precursors were designated as C-Y, where Y represents the specific carbonization temperature.

Chemical activation

The biocarbon produced at 500 °C (C-500) was selected for chemical activation. The precursor was impregnated with potassium hydroxide (KOH) solution at specific mass ratios (1:1, 3:1, 5:1, 7:1 KOH:biomass). The mixture was dried and subsequently underwent thermal activation in the same tubular furnace under a nitrogen atmosphere. Based on optimization for maximum surface area and pore volume, the activation was

conducted at 800 °C for a holding time of 120 min (Muratov et al., 2025).

The reactor configuration included dedicated exhaust ports for the efficient removal of condensable liquids (bio-oil) and non-condensable gaseous by-products generated during pyrolysis. The activated carbon products were labeled ACX-800, where X denotes the KOH/carbon mass ratio.

Characterization of sample

Comprehensive physicochemical analysis was performed on both the raw licorice root residues and the synthesized activated carbons. All experimental measurements were conducted in triplicate to ensure statistical reproducibility.

Ash content was determined following ASTM D3174-04, and volatile matter was measured in accordance with ASTM D3175-89a. The elemental composition (C, H, N, and S) was quantified via high-temperature combustion using a FLASH-2000 Elemental Analyzer (Thermo Fisher Scientific, Germany) according to ASTM D5291-96. The oxygen content was calculated by difference:

$$O\,(\%) = 100 - (C + H + N + S + Ash) \qquad (1)$$

Calorific value: The gross calorific value (GCV) was determined using an oxygen bomb calorimeter in compliance with ASTM D240-02 (Ibrahim et al., 2010).

X-ray phase analysis was performed using an XRD Empyrean PANalytical X-ray diffractometer (Boston, USA) with a scan range of 5° to 80° at a scan speed of 2°/min and angle reproducibility of < 0.01° (Khurmamatov et al., 2024).

Elemental composition and quantitative content of elements were determined using an energy-dispersive X-ray (EDX) fluorescence spectrometer. Scanning electron microscopy (SEM) was used to analyze the surface morphology of the initial sample and its treatment products, employing the EVO MA10 SEM microscope (Tokyo, Japan), which also provided elemental composition data.

Infrared spectra were recorded on an Avatar 360 FT-IR Nicolet iS50 Thermo Fisher Scientific spectrometer (Tokyo, Japan) within a frequency range of 4000-400 cm^{-1} (Muratov et al., 2024). Under high-purity nitrogen purge (flow rate: 50 mL/min), thermogravimetric and differential thermal analyses were conducted using a Q-1500 D derivative gravimeter (Tokyo, Japan). The sample mass was precisely controlled at 10 ± 0.5 mg, heated from 30 °C to 900 °C at a ramp rate of 10 °C/min in an open platinum crucible.

Textural and adsorption characteristics

The porous structure characteristics, including specific surface area, total pore volume, and pore diameter, were determined using low-temperature N_2 adsorption at 77 K on an Autosorb IQ Quantachrome Nova 1000e system (Tokyo, Japan). Samples were vacuum-treated at 150 °C for 12 h before analysis. Relative pressure was set to 0.995 P/P_0, with adsorption/desorption isotherms measured from 0.05 to 0.995 P/P_0.

The BET method was used to process the adsorption curves, while the *t*-Plot method determined the micropore volume. The mesopore volume was calculated by subtracting the micropore volume from the total volume. The average pore diameter was calculated using the BET method ($D = 4\ V/S$), and micropore volumes and size distribution (average size ≈ 1.15 - 1.17 nm) were assessed using the Horvath-Kawazoe (HK) method (Kalbaev et al., 2026).

Batch adsorption test

Adsorption performance of the material was tested using methylene blue (MB) solutions, with adsorption isotherms obtained at varying temperatures and concentrations. Adsorbed amounts were analyzed using the BET and Langmuir equations. Quantitative analysis was performed using a UV/V-5100 spectrophotometer (Shanghai Metas, China), measuring the absorbance in the range between 190 and 700 nm. MB adsorption capacity was determined by measuring absorbance at 660 nm. All experiments were conducted at 25 °C for a duration of 2 hours.

For adsorption capacity experiments, methylene blue (MB) dye solutions were prepared, and their absorbance was measured to construct a calibration curve. Then, 0.05 g of powdered activated carbon samples were added to 50 mL of each dye solution concentration. The flasks were gently shaken until an equilibrium was reached, as determined by adsorption kinetics. After equilibrium, the absorbance was measured, and its concentrations were calculated using the calibration curve. The amount of adsorbed dye is determined by Equation 2:

$$A = \frac{(C_0 - C_1) \times V}{m} \quad (2)$$

where: A is the amount of adsorbed adsorbate (mmol/g); C_0 and C_1 are the initial and equilibrium concentrations of adsorbate in the solution (mmol/L); V is the volume of the solution (L); m is the mass of the adsorbent (g).

The Langmuir and Freundlich isotherms were fitted to experimental data to understand adsorption mechanisms (Table 1).

RESULTS AND DISCUSSIONS

Thermochemical evolution and yield dynamics

Thermogravimetric analysis (TGA) and differential thermal analysis (DTA) provided insights into the pyrolytic decomposition of licorice root residue (Figure 1).

Thermal analysis of licorice root residue, Figure 1 revealed key transformations at various temperature intervals. At 110–120 °C, it was found that desorption of physically adsorbed water caused 2.25% of mass reduction. A significant mass loss began at 206 °C, indicated by a marked change in the thermogram profile, signifying further material breakdown.

Between 206 °C and 310 °C, the most significant decomposition of organic compounds occurred, resulting in a 20–22% mass loss due to the thermal breakdown of hemicellulose and the release of chemically bound functional groups. As the temperature increased from 310 °C to 500 °C, the mass reduction reached 57%, driven by the decomposition of cellulose and the initiation of lignin carbonization, which involves the evolution of volatiles such as CO and CO_2. Further degradation between 510 °C and 900 °C accounted for an additional 8.0% loss, linked to the slow volatilization of residual carbonaceous matter and the consolidation of the inorganic fraction.

Table 1. Equations of Langmuir, Freundlich, Temkin and Dubinin-Radushkevich models

No	Models	Formula	Explanation
1	Langmuir	$\frac{1}{q_e} = \frac{1}{K_L \cdot q_{max}} \cdot \frac{1}{C_e} + \frac{1}{q_{max}}$	q_e – maximum adsorption capacity (mg/g), K_L– Langmuir constant.

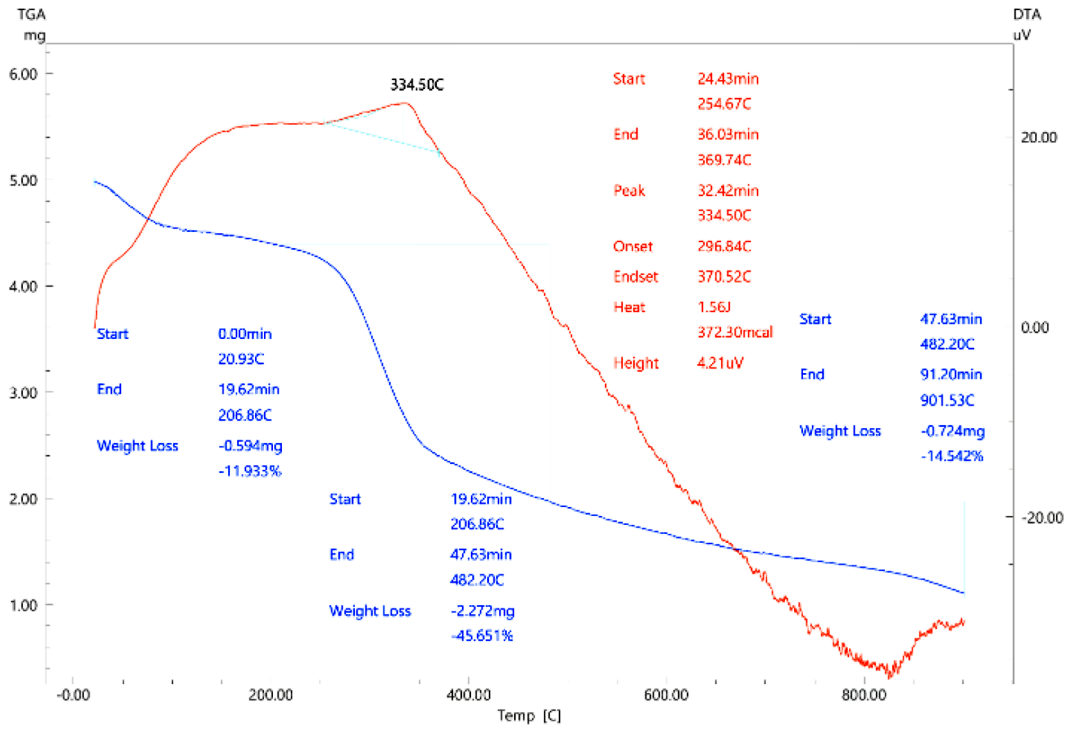

Figure 1. Thermogram of licorice root residue

Table 2. Variation of mass changes (%) of carbonized material as a function of temperature at varying time (h)

Hours	Carbonization temperature, °C						
	400	500	600	700	800	900	1000
1	48.02	49.04	56.21	61.24	70.24	73.05	76.89
2	58.10	59.20	60.50	68.00	71.90	74.20	81.24
3	58.12	59.22	60.51	68.34	71.94	74.23	79.87
4	58.56	59.70	61.05	69.12	72.45	75.08	79.51
5	59.14	60.25	61.55	69.98	72.93	75.83	79.25

Comprehensive analysis indicates that the pyrolysis of licorice root residues for the synthesis of effective adsorbents should be performed at temperatures of at least 500 °C. At this thermal threshold, the significant decomposition of organic precursors and the stabilization of the carbon matrix occur. Reaching these temperatures ensures the removal of volatile matter and the enhancement of the structural properties necessary for high-capacity adsorption.

The structural and chemical transformations of licorice root residues during thermal treatment were investigated as a continuation of prior thermal analysis. Particular attention was given to both quantitative and qualitative changes. Table 2 presents the mass variations observed during carbonization, depending on temperature and treatment duration. Table 2 illustrates the mass changes during carbonization as a function of temperature and duration.

As shown in Table 2, mass loss is highly sensitive to the carbonization temperature, with the most aggressive reduction occurring within the first 2 hours. This corresponds to the TGA data where the collapse of the lignocellulosic framework releases CO and CO_2, leaving behind a stable carbonaceous skeleton.

For longer durations, higher mass loss percentages were evident, but the differences between these durations were less pronounced. This suggests a threshold duration beyond which additional time resulted in diminishing returns in mass loss..

Table 3 shows that as the temperature increased, the yield of biocarbon decreased from 41.9% at 400 °C to 21.1% at 1000 °C. This indicates more intensive decomposition of organic material at higher temperatures. The maximum yield of liquid was observed at 700 °C (23.3%), after which its value began to decrease. This might indicate that at higher temperatures, liquid components decompose or transition into the gaseous phase. The yield of gaseous products increased with rising temperature from 43.3% at 400 °C to 54.4 % at 900 °C. This suggests that high temperatures promoted the gasification of carbon-containing substances.

Volatile matter in carbon ranged from 21.5% at 400 °C to 32.6 % at 900 °C. This implies that as the temperature increased, the volatile components of carbon burned off intensively, leaving a more stable carbon residue. The ash content of carbon increased with the rise in processing temperature, starting from 10.7% at 400 °C and reaching 19.9% at 900 °C. This might be related to the concentration of inorganic components in the carbon after the thermal decomposition of the organic matter.

The ash remains after the combustion of organic material provides insight into the composition of the original material (Paryanto et al.,

Table 3. Yield of various products during 2 h of licorice root residue pyrolysis

T, °C	Product yield (%)			Volatile matter in biocarbon, (%)	Ash content of biocarbon, %
	Biocarbon	Liquid	Gas		
400	41.9	14.8	43.3	21.5	10.7
500	40.8	16.3	42.9	21.1	11.8
600	39.5	17.8	42.7	20.9	14.2
700	32.0	23.3	44.7	22.9	15.5
800	28.1	21.2	50.7	28.9	17.9
900	25.8	19.8	54.4	32.6	19.9

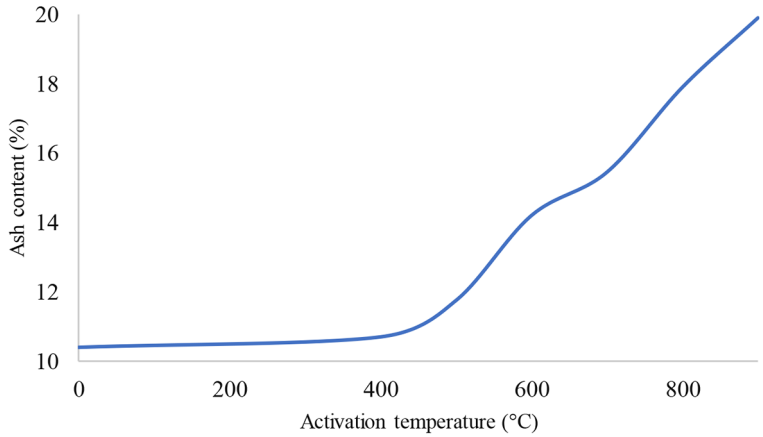

Figure 2. Quantitative dependency of ash content in carbonized material on activation temperature

2019). Figure 2 shows that the ash content increased with higher activation temperatures. Initially, the ash content in licorice root residues was 10.4%. At 400 °C, the ash fraction slightly rose to 10.7%, indicating the beginning of structural changes in the licorice root residue.

With the pyrolysis temperature raised to 500 °C, the ash content increased to 11.75%, reflecting continued thermal decomposition of organic components and the release of mineral elements. At 600 °C, the ash content significantly increased to 14.2%, confirming the active transformation of organic substances into inorganic residue.

The most notable increase in ash content occurred between 700 °C and 900 °C, where it rose from 15.5% to 19.9%. This suggests that higher activation temperatures led to a progressive increase in ash residue due to the loss of volatile organic components and the formation of new mineral structures. Table 3 presents the results of the pyrolysis of licorice root residue at varying temperatures.

In the experiment, carbonized materials formed at 500 °C were also analyzed to assess the impact of KOH solution on their properties. Figure 3 shows the changes in the ash content after chemical activation for 20 h.

Further research indicated that similar results could be achieved within 4 h by increasing the activation temperature to 100 °C, with an optimal limit of 120 °C. This suggests that the chemical activation process could be optimized for enhanced efficiency and time savings. In the investigation of KOH's effect on carbonized material obtained at 500 °C (AC-500), a significant reduction in the ash content from 17.9% to 4.35% was observed, indicating the solution's high efficiency in leaching mineral components. However, when the mass ratio of KOH solution to carbonized material reached 7:1, the ash

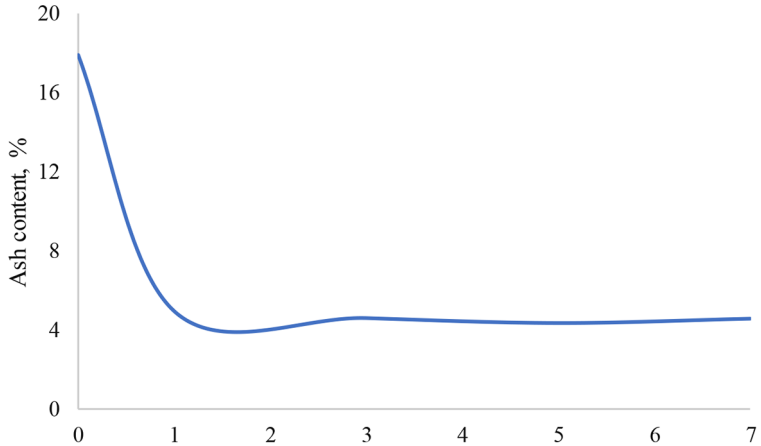

Figure 3. Correlation between ash content and the mass ratio of KOH to the carbonization product during activation

content slightly increased to 4.57%. This minor increase might be due to secondary precipitation of soluble mineral components, which could stem from the changes in the solubility or solution saturation leading to partial recrystallization and increased ash content (Ramamoorthy et al., 2020). The conditions affect the porous structure of the materials.

The results suggest that the optimal KOH solution to carbonized product mass ratio for minimizing ash content ranged between 1:1 and 5:1. Beyond this range, the leaching efficiency decreased, causing a higher ash content. The yield decreased with higher KOH solution flow rates at a 1:1 ratio (AC1-800), the yield was 22.9%, whereas at ratios of 1:3, 5, and 7 (AC3-500, AC5-500, and AC7-500), the yields were 22.2%, 21.8%, and 21.3%, respectively. This highlights the need to control KOH concentration during purification to achieve optimal results.

Characterization of samples

X-ray diffractograms of the samples were studied. The comparative results are presented in Figure 4. Figure 4 shows that the peaks at 2θ in the X-ray diffractograms of carbons indicate the presence of graphite-like structures and amorphous carbon. In carbons with various degrees of metamorphism, a peak around 20–30°

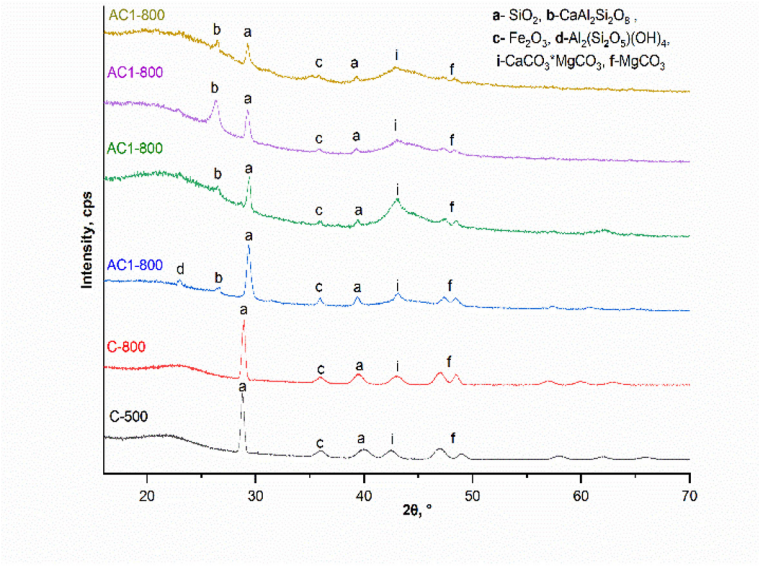

a)

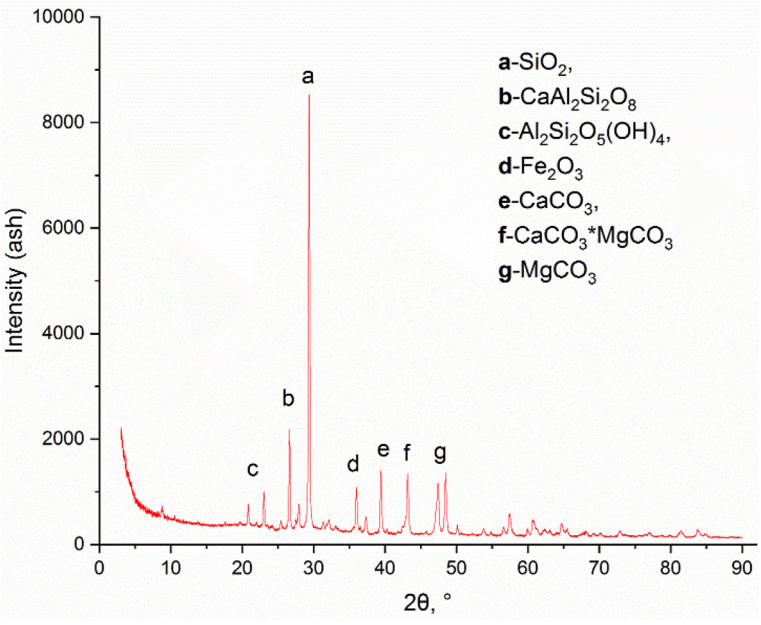

b)

Figure 4. X-ray diffractograms of samples: (a) biocarbons and (b) ash fraction of licorice root residue

(2θ) corresponds to the (002) plane of graphite, suggesting a layered carbon structure. The peak around 40–45° (2θ), related to the (100) or (101) planes, was associated with the interplanar distance in aromatic layers. A broader, less intense peak around 15–25° (2θ) indicates amorphous carbon and a low degree of graphitization.

Comparing the X-ray diffractograms of three different carbon samples (AC1-800, AC3-800, AC5-800 and AC7-800), thermally activated at 800 °C after chemical activation with KOH, revealed distinct structural changes. The AC1-800 sample showed characteristic peaks (2θ) at 29.18°, 26.37°, and 42.91°, indicating certain crystalline phases. The AC5-800 sample displayed changes in peak intensity and position compared to the original carbonized sample, reflecting structural changes due to KOH treatment. Peaks (2θ) at 29.26°, 26.47°, and 39.27° suggest new porous structures.

The AC5-800 sample showed more pronounced changes with strong peaks at 26.15, 43.47, and 64.16°, indicating the formation of specific structural features due to thermal treatment. According to previous studies (Wu and Zhang, 2019), thermal and chemical activation processes significantly altered carbon's structure, developing porous structures and functional groups that enhance adsorption properties. The diffractograms suggest that the AC3-800 samples had an amorphous character, while the AC5-500 sample showed changes before and after treatment due to chemical activation, and the AC7-800 exhibited pronounced crystalline peaks, indicating a higher degree of crystallinity.

By analyzing the X-ray diffractogram of the carbon ash fraction in Figure 4b, while comparing the 2θ peaks and their corresponding *d*-spacing with standard X-ray diffraction data, it is evident that higher and narrower peaks indicate larger and more ordered crystalline phases. The peak with the highest intensity (I/II = 100) at 29.1815° and *d* = 3.05780 Å likely corresponded to quartz (SiO_2), a common mineral in carbon ash.

The ash also contained muscovite or illite with its peaks around 26.4463° and 39.2239° (2θ), indicating layered silicates and hematite, or magnetite with its peak around 64.5487° (2θ), corresponding to iron oxides. The porosity of activated carbons stems from three primary sources: the internal cell structure of the original material, the charcarbon preparation conditions, and the starting material's composition.

Scanning electron microscopy (SEM) allows for observing the surface topography of carbons, crucial for determining pore shape and orientation. SEM also can track changes in the starting material during activated carbon production, enhancing the understanding of pore development (Achaw, 2012). The study of the surface morphology of carbon samples derived from licorice root residue indicated that thermal treatment and chemical activation altered the porous structure and the quantitative content of major elements, such as carbon (Figure 5 and Table 4).

Figure 5 illustrates the surface morphology and pore structure of the carbonized and activated samples. The SEM image of the carbonized sample (C-500) shows irregular, broken particles with relatively smooth surfaces and limited visible porosity, indicating the initial stage of pore development.

Thermal activation at 800 °C, significant changes in morphology are observed. The C-800 sample exhibits the formation of a porous structure, although pore development remains relatively limited. With chemical activation KOH, the AC3-800 and AC5-800 samples show progressively more developed and well-defined porous networks, indicating enhanced activation and pore formation.

The AC5-800 sample demonstrates the most developed and uniform porous structure, which is consistent with its highest surface area and pore volume reported in Table 5. In contrast, the AC7-800 sample shows signs of structural deterioration, likely due to overactivation, which can lead to partial pore collapse or blockage.

These observations are consistent with textural analysis results, confirming that both thermal and chemical activation significantly enhance porosity. The evolution of pore structure with increasing KOH ratio reflects the balance between pore formation and destruction, with optimal development observed at a ratio of 1:5.

Table 4 shows a significant increase in carbon content from the C-500 carbonized sample to the thermoactivated samples AC3-800 and AC5-800, indicating that activation at 800 °C enhanced carbon content, likely improving the carbon's adsorption properties. The AC3-800 and AC5-800 displayed a notable reduction in oxygen content, as compared to C-500 and C-800. This reduction likely resulted from the thermal breakdown of oxygen-containing groups during high-temperature processing. The original C-500 sample contained elements such

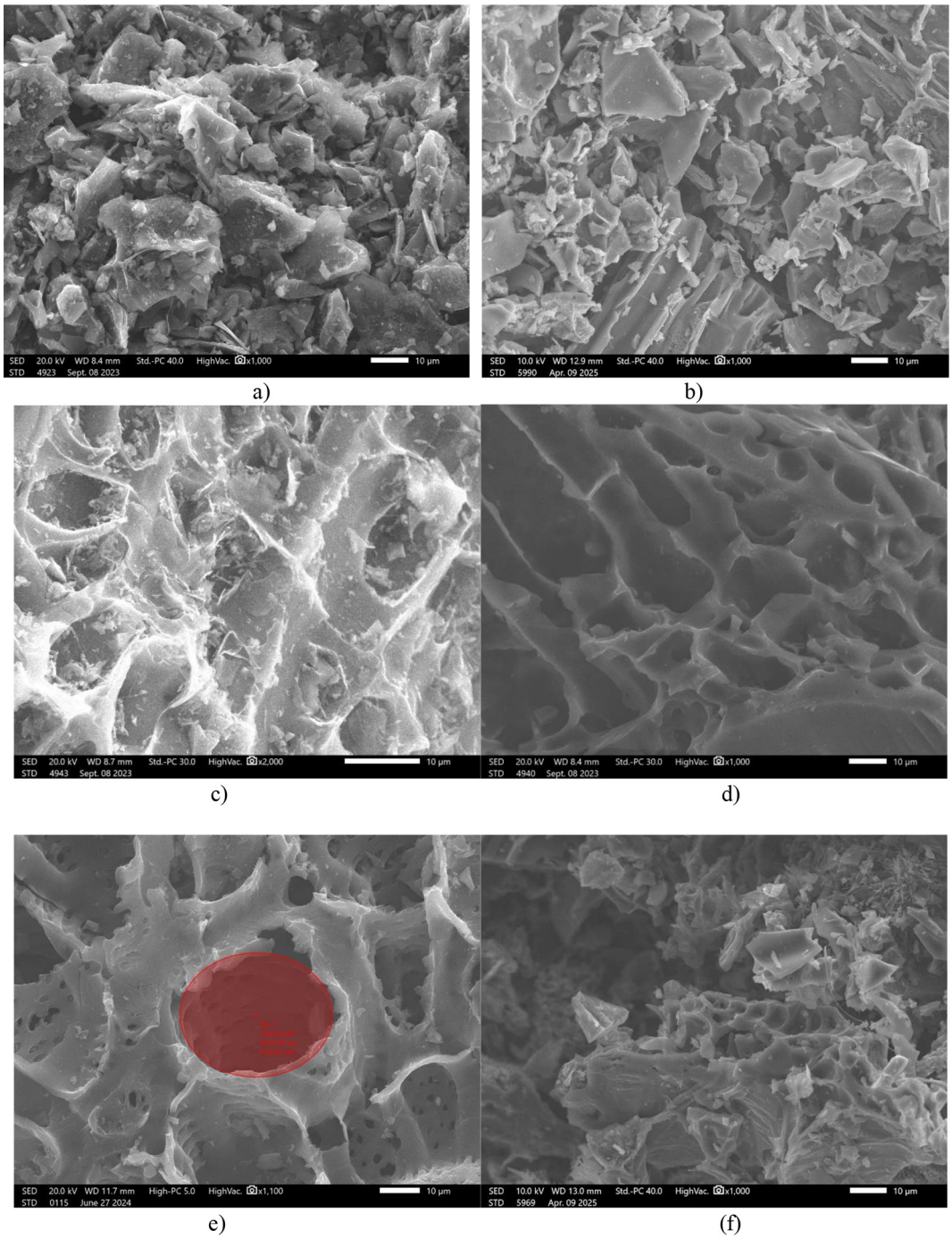

Figure 5. SEM images of samples: (a) C - 500; (b) C-800; (c) AC1 – 800; (d) AC3 – 800; (e) AC5 – 800 and (f) AC7-800

as Na, Mg, Si, P, S, Cl, K, Ca, Al, and Fe, which were diminished or absent in the activated samples, suggesting that activation removed certain inorganic impurities. The sample AC5-800, with higher carbon content and lower oxygen content than the C-800, indicates that activation not only changed the chemical composition, but also enhanced the carbon's porosity and adsorption efficiency.

Figure 6 shows minor differences in the infrared (IR) spectra with respect to absorption intensity. The activated carbons exhibited significantly higher band intensities, as compared to the carbonized material obtained at 500 °C. The OH group peak shifted from 3445 cm^{-1} in the carbonized material to 3435 cm^{-1} (for the AC3-800) and 3426 cm^{-1} (for the AC5-800) in KOH-activated samples. Although thermal activation

Table 4. Elemental analysis of carbon samples

Elements	Elements in each sample (%)					
	C - 500	C-800	AC1-800	AC3 - 800	AC5 - 800	AC7-800
C	77.78	79.55	93.77	94.37	97.91	97.28
O	13.26	11.45	4.32	4.05	0.98	1.2
Na	0.51	0.26	0.12	-	-	–
Mg	0.90	0.78	0.24	0.25	–	–
Si	0.32	5.16	–	0.30	0.28	0.24
P	0.21	0.22	–	-	-	–
S	0.15	0.11	–	-	-	–
Cl	0.42	0.42	–	-	-	–
K	2.84	1.64	0.42	0.38	0.20	0.44
Ca	2.63	0.68	0.51	0.45	0.42	0.42
Al	0.48	0.22	0.11	0.09	-	0.24
Fe	0.52	0.61	0.13	0.11	0.18	0.18

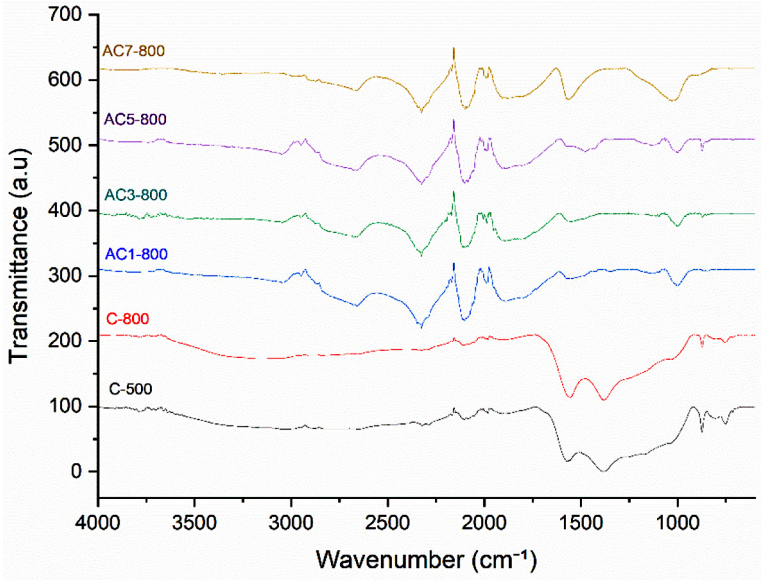

Figure 6. FT-IR spectra of carbons

did not significantly change the peak positions, it reduced their intensity, indicating fewer -OH groups after thermal treatment of chemically activated samples. In the AC1-800, the peaks at 2922 and 2852 cm^{-1} corresponded to the C-H bonds in alkyl chains, while the 1618 cm^{-1} peak suggested C=C bonds, found in aromatic rings. The 1384 cm^{-1} peak indicates symmetric bending of C-H groups, and the 1032 cm^{-1} peak implied C-O bonds typical of ethers or alcohols.

For the AC3-800, the spectrum showed peaks at 3430 cm^{-1} (OH groups), 2924 and 2853 cm^{-1} (C-H bonds), 1634 cm^{-1} (C=C or C=O bonds), 1384 cm^{-1} (C-H bonding), and 1033 cm^{-1} (C-O bonds). These spectra indicate that the main absorption peaks remained unchanged, preserving the primary chemical groups in the sample. Slight changes in intensity and peak positions implied changes in the functional groups' environment due to interaction with KOH or structural changes in the carbonized material.

Comparing the AC5-800 with the previous samples, the 2924 and 2854 cm^{-1} peaks were less pronounced, indicating transformations in alkyl chains. The 1635 cm^{-1} peak was more intense and sharper, suggesting an increase in carbonyl groups or higher conjugation in the carbon material. These changes resulted from KOH treatment,

leading to additional oxidation and modification of the carbon's chemical structure.

Texture characteristics

The temperature of the carbonization process significantly influences the porous structure of the materials. Figure 7 shows nitrogen adsorption isotherms for carbonized materials obtained at varying temperatures. These isotherms (Figure 7) were hybrids of Type I (sharp increase in adsorption at $P/P_0 < 0.05$, typical of microporous solids) and Type IV (hysteresis loop formation at moderate and high pressures).

Carbon activation with KOH enhanced specific surface area, porosity, and pore distribution (Ghorbani et al., 2020b). It was obvious from Figure 8 that isotherms of all four samples belong to type IV, indicating mesopore filling with a plateau at high relative pressures. The AC5-800 and AC3-800 exhibited higher adsorption capacities than the AC1-800 and AC7-800, suggesting more adsorbed

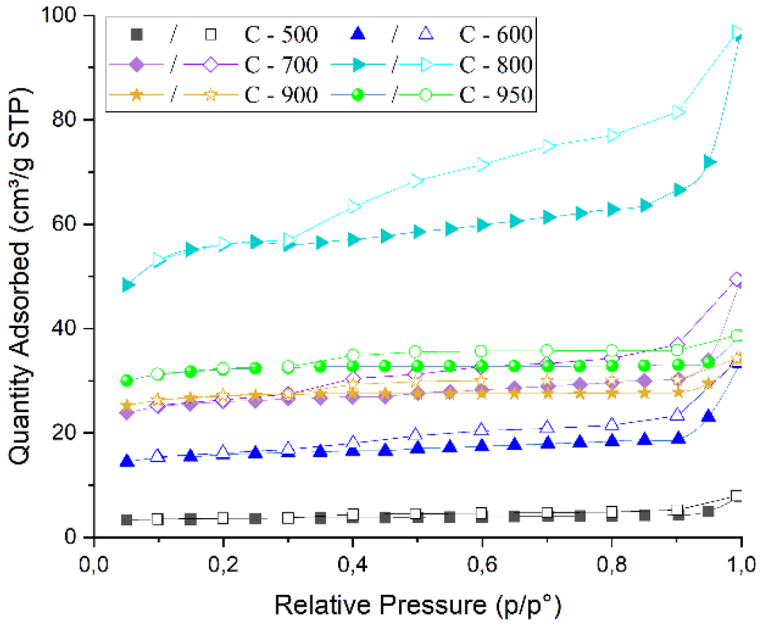

Figure 7. N_2 adsorption/desorption isotherms on carbonized materials obtained at varying temperatures

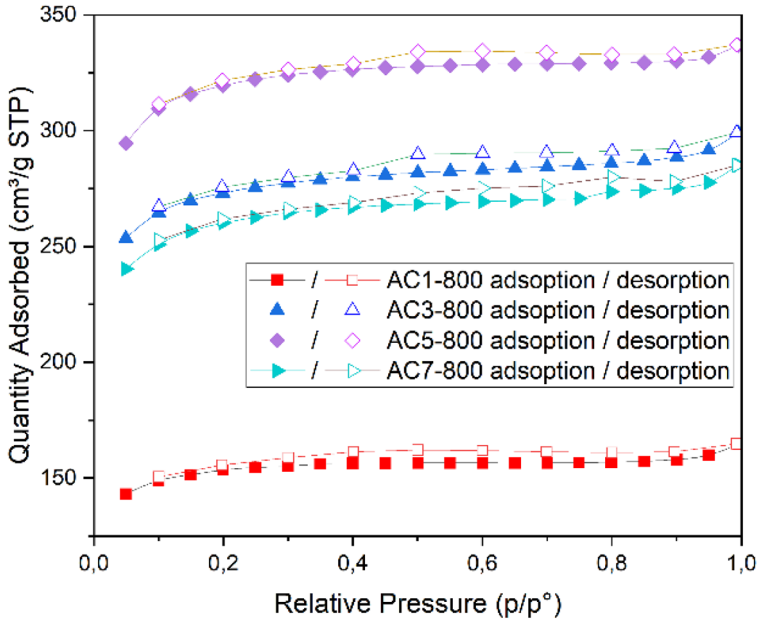

Figure 8. Nitrogen adsorption and desorption isotherms on thermochemical activated samples

Table 5. Textural characteristics of samples

Sample	S^1 (m^2/g)	S^2 (m^2/g)	*t*-Plot* (m^2/g)	V_a (cm^3/g)	V_b (cm^3/g)	R (Å)
C - 500	11.18	17.54	2.89	0.0043	0.0038	49.86
C - 600	49.45	77.96	12.96	0.0187	0.0174	49.44
C - 700	80.71	125.98	18.09	0.0321	0.0252	50.54
C - 800	169.81	266.63	53.99	0.0627	0.0635	48.30
C - 900	77.52	121.10	15.33	0.0350	0.0116	56.96
C - 950	98.98	144.01	18.24	0.0420	0.0136	56.94
AC1 - 800	447.40	698.93	87.44	0.2340	0.2543	22.11
AC3 - 800	799.67	1283.20	166.89	0.4180	0.4591	22.53
AC5 - 800	917.69	1451.20	203.36	0.4870	0.5167	22.21
AC7 - 800	837.77	1333.00	185.26	0.3960	0.4784	22.37

Note: S^1 – specific surface area by BET; S^2 – specific surface area by Langmuir; * – external surface area; V_a – micropore volume; V_b – mesopore volume; R – median pore width.

substance at the same relative pressures. Th e steep initially rose in all curves implies micropores, with adsorption increasing with relative pressure, typical of physical adsorption. Increasing KOH amount boosted the adsorbent's adsorption capacity, consistent with textural characteristics showing larger specific surface area and pore volume with higher carbonized material to KOH ratios.

The textural properties presented in Table 5 enable a direct comparison between thermal activation and chemical (KOH-assisted) activation, highlighting fundamental differences in pore development mechanisms. Thermally activated samples (C-500 to C-950) exhibited a gradual increase in specific surface area with temperature, reaching a maximum at 800 °C (169.81 m^2/g), followed by a decline at higher temperatures. This trend indicates that thermal activation alone promotes pore formation primarily through the decomposition of volatile components and gradual development of the carbon matrix. However, excessive temperatures (≥900 °C) lead to structural degradation, including pore widening, merging, and partial collapse, which reduces both micropore and mesopore volumes.

In contrast, chemical activation with KOH resulted in a substantially more developed porous structure, with surface areas increasing dramatically from 447.40 m^2/g (AC1-800) to 917.69 m^2/g (AC5-800). This demonstrates that chemical activation is significantly more effective in generating porosity than thermal treatment alone. The enhancement can be attributed to the dual role of KOH, which not only facilitates carbon etching and pore creation but also removes inorganic components, thereby increasing accessible surface area and pore volume. Unlike thermal activation, where pore formation is mainly governed by temperature, chemical activation introduces an additional parameter—activating agent concentration—which allows more precise control over pore structure.

A key distinction between the two processes lies in pore size distribution evolution. Thermal activation showed limited development of microporosity and mesoporosity, with relatively low V_a and V_b values even at optimal temperature. Conversely, chemical activation significantly increased both micropore and mesopore volumes, indicating the formation of a hierarchical pore structure. This is particularly evident in the AC5-800 sample, where balanced micro–mesoporous development was achieved, which is desirable for adsorption applications involving molecules of different sizes.

However, the results also reveal a critical limitation of chemical activation. Increasing the KOH ratio beyond the optimal level (AC5-800) resulted in a decline in specific surface area and pore volume (AC7-800), indicating over-activation. This phenomenon is associated with excessive carbon burn-off, pore wall thinning, and eventual pore collapse or blockage. In contrast to thermal activation, where structural degradation is primarily temperature-driven, chemical activation is more sensitive to reagent concentration, making process optimization essential.

Overall, while thermal activation provides a simpler and more stable pathway for carbon structure development, its ability to generate

high surface area and well-developed porosity is limited. Chemical activation, on the other hand, is markedly more efficient in enhancing textural properties, producing carbons with significantly higher surface area and pore volume. Nevertheless, its effectiveness is constrained by the risk of over-activation, emphasizing the need for careful control of KOH concentration. These findings confirm that thermochemical activation offers superior performance compared to purely thermal treatment, but only within an optimal activation window.

The pore size distributions of the samples according to N_2 adsorption-desorption isotherms are shown in Figure 9.

It can be seen from Figure 9 that during the initial activation phase with a carbon-to-KOH ratio of 1:1, the porous structure was dominated by micropores (diameters smaller than 2 nm). The cumulative pore volume reached 0.24 cm^3/g, with micropores accounting for the majority of the porosity. Mesopores (diameters between 2–50 nm) were minimal, indicating that low KOH concentrations primarily facilitate the formation of narrow pores, suitable for adsorbing small molecules. Increasing the ratio to 1:3 resulted in a substantial increase in pore volume, with the cumulative volume nearly doubling to 0.44 cm^3/g. At this stage, mesopore formation began, signifying an expansion in the pore size distribution and the development of a more diverse porous structure. The optimal porosity was achieved at a carbon-to-KOH ratio of 1:5, where the cumulative pore volume peaked at 0.48 cm^3/g. This ratio promoted a balanced development of both micropores and mesopores, resulting in a well-distributed porous structure. The enhanced fraction of mesopores at this stage made the material particularly effective for adsorbing molecules of varying sizes.

The observed reduction in adsorption capacity and surface area at the highest KOH/carbon ratio (1:7) is a characteristic result of starting point of over-activation. While KOH facilitates pore formation through the etching of the carbon matrix, an excessive concentration leads to a secondary reaction where the pore walls become too

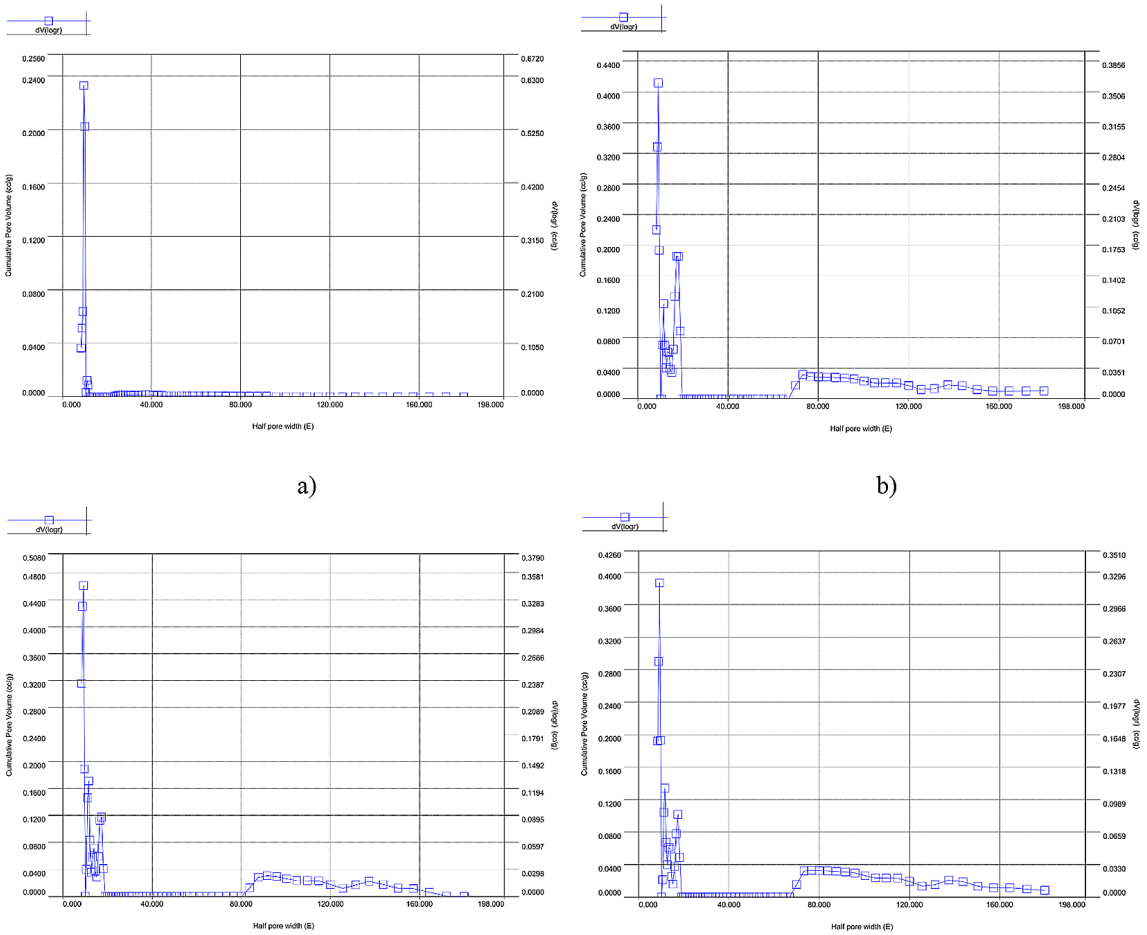

Figure 9. The pore size distributions of: (a) AC1 – 800, (b) AC3 – 800, (c) AC5 – 800, (d) AC7 – 800

thin and eventually collapse. This structural degradation results in the merging of micropores into larger, less effective voids or the complete blockage of pore entries by redistributed carbonaceous matter, thereby reducing the available specific surface area for methylene blue molecules (Luo et al., 2020; Wijewardhana et al., 2026).

However, further increasing the KOH ratio to 1:7 led to a slight reduction in the cumulative pore volume to 0.42 cm^3/g. This decline is likely due to pore destruction or redistribution caused by excessive activation, a phenomenon known as overactivation. Such overactivation can compromise the material's overall porosity, diminishing its effectiveness as an adsorbent (Harimisa et al., 2022) (Figure 10).

Adsorption of methylene blue (MB) on samples

The adsorption isotherms of MB on the studied adsorbents are presented in Figure 11.

Figure 11 demonstrate that thermal treatment temperature significantly influences the initial adsorption characteristics of the biocarbons. The C-800 sample shows a higher adsorption capacity

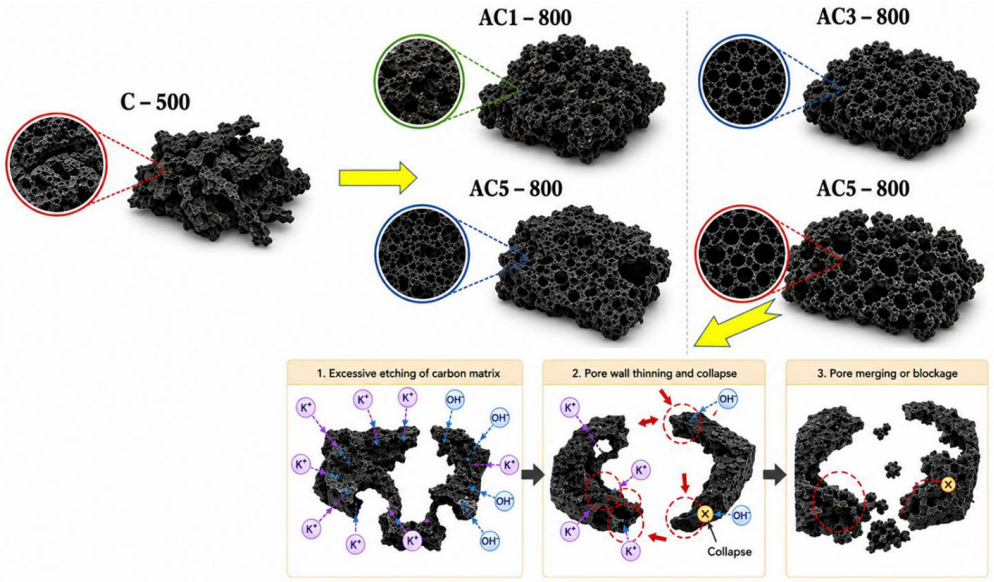

Figure 10. Evolution of pore structure in KOH-activated carbon showing progressive etching, pore wall thinning, collapse, and pore merging with increasing activation severity

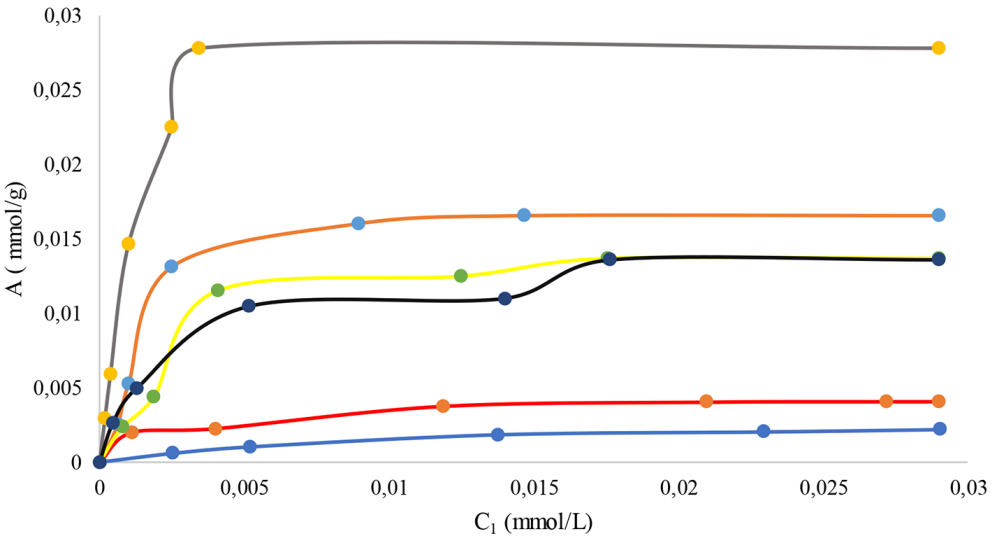

Figure 11. Adsorption isotherms of MB on the studied adsorbent (Legend: Blue line: C-500, Red line: C-800, Yellow line: AC1-800, Orange line: AC3-800, Gray line: AC5-800, Black line: AC7 -800)

at the initial stage compared to the C-500, suggesting that increasing the carbonization temperature to 800 °C enhances the primary pore development and surface functionalities favorable for dye uptake. However, both samples eventually reached a plateau at relatively low concentrations, indicating a limited number of available adsorption sites compared to chemically activated samples.

Specifically, while C-800 achieved a higher saturation level than C-500, its performance remained constrained by a relatively low specific surface area of 169.81 m²/g, as shown in Table 5. This confirms that while thermal activation at 800 °C is superior to 500 °C for creating a stable carbon matrix, it is insufficient on its own to produce the high-capacity porosity required for maximum methylene blue removal. Chemically activated samples (AC1-800, AC3-800, AC5-800, AC7-800) generally displayed higher adsorption capacities compared to the thermally activated samples prepared at 500 °C and 800 °C. This indicates that KOH activation significantly enhanced pore development, increased specific surface area, and improved the accessibility of adsorption sites, thereby promoting adsorption performance.

This analysis highlights the strong influence of both thermal and chemical activation on the adsorption properties of activated carbons derived from licorice root residue. In particular, the chemically activated samples exhibited superior adsorption behavior, suggesting their greater suitability for applications such as dye removal from aqueous solutions. The observed differences among the samples emphasize the importance of optimizing activation conditions, including temperature and activating agent ratio, to maximize adsorption capacity and overall efficiency.

The correlation coefficients (R^2) were used to assess the suitability of applying the equations for each adsorbent. From the adsorption isotherm data, the Langmuir constant and other parameters describing the surface properties of these carbon materials were determined (Table 6). Analysis of Table 6 reveals significant variations in the textural characteristics and adsorption behavior of the prepared carbon adsorbents. A clear structure–property relationship is observed for the AC1-800 to AC5-800 series, where an increase in BET specific surface area from 447.40 to 917.69 m²/g is accompanied by a proportional rise in methylene blue (MB) adsorption capacity. This trend confirms that surface area is a dominant factor governing adsorption performance in these hierarchical porous structures.

In addition to surface area, the Langmuir constant (K), which reflects adsorbent–adsorbate affinity, also varies considerably among samples. For example, C-800 exhibits a higher K value compared to C-500, indicating improved adsorption affinity at higher activation temperature. Notably, AC7-800 shows the highest Langmuir constant (438.791), suggesting the strongest interaction with methylene blue among all samples, despite not following the same surface area trend.

However, adsorption behavior cannot be explained by surface area alone. Although AC7-800 possesses a relatively high theoretical surface area, its reduced pore volume and less accessible internal structure limit diffusion of relatively large dye molecules such as methylene blue (approximate molecular dimensions 1.43 × 0.61 × 0.40 nm). This makes pore size distribution and connectivity equally critical alongside total surface area in determining adsorption efficiency.

The total pore volume further supports these observations, with AC5-800 showing the highest value (0.0497 cm³/g), consistent with its favorable adsorption of larger molecules. Meanwhile, the correlation coefficient (R^2) values for most samples, including C-500 and C-800 (99.5% and 99.3%, respectively), confirm that the Langmuir isotherm adequately describes the adsorption process across these materials.

Table 6. Comparison of textural characteristic indicators based on methylene blue adsorption

Sample	*K*	Surface area, (m²/g)	*ΣV* (cm³/g)	R^2 (%)
C-500	107.61	1.83	0.0029	99.5
C-800	405.62	2.81	0.0045	99.3
AC1-800	233.03	10.83	0.0171	96.7
AC3-800	342.47	12.89	0.0204	96.6
AC5-800	359.29	31.42	0.0497	96.9
AC7-800	438.79	9.026	0.0143	97.7

This could be explained due to the fact that activated carbons derived from different precursor materials, such as licorice root residue and carbon, exhibited distinct physical and chemical properties, such as surface area, pore structure, and surface functionality. By comparing the characteristics of licorice root-derived activated carbon with those of carbon-derived activated carbon, this work aimed to highlight the advantages and limitations of using biomass residues as sustainable alternatives to traditional fossil-based precursors.

The carbon samples serve as a benchmark due to their well-documented performance in applications, such as adsorption and catalysis. By referring to the properties of carbon-derived activated carbon, this work demonstrates that licorice root residue-derived activated carbon exhibited a comparable or superior performance with respect to adsorption capacity, specific surface area, pore size distribution.

While this study focuses on the initial adsorption performance, the regenerability of licorice root-based activated carbon is a vital factor for industrial viability. Previous research suggests that biomass-derived carbons can be regenerated via thermal treatment or solvent washing (e.g., ethanol or acidic solutions) to desorb organic dyes. However, repeated regeneration cycles typically result in a 50% decrease in efficiency due to the progressive loss of surface functional groups and the accumulation of residual adsorbate within the micropores, a factor that requires further long-term stability testing for this specific material (Liyanaarachchi et al. 2023). Highlighting the differences between activated carbon from licorice root residue and carbon also underscores the environmental and economic benefits of utilizing agricultural waste as a precursor. Unlike carbon, licorice root residue is a renewable and abundant resource, offering a more sustainable pathway for activated carbon production. This comparison emphasizes the broader implications of this work in promoting waste valorization and reducing reliance on non-renewable resources.

Despite its effectiveness, the thermochemical activation approach employed in this study presents two main limitations. First, the process is highly sensitive to the activating agent-to-carbon ratio, where deviations from the optimal KOH loading can lead to excessive etching and pore wall thinning. At higher ratios (e.g., AC7-800), this over-activation may result in partial pore coalescence and structural degradation of the carbon framework, as suggested by the reduced surface area and adsorption performance. Second, the method requires high-temperature treatment (800 °C) under an inert atmosphere (N_2), which increases energy consumption and operational complexity compared to lower-temperature physical activation routes, thereby potentially increasing process cost and environmental burden.

CONCLUSIONS

This study has successfully optimized the production parameters for creating activated carbon (AC) from licorice root residue, a biomass waste generated by the herbal processing industry. By systematically adjusting carbonization temperature, KOH concentration, and activation time, this work has provided insights into how these factors influence the development of porous structure and adsorption performance. The application of thermochemical activation using KOH proved effective in enhancing surface area and tailoring pore size distribution, which in turn improved the material's adsorption capabilities.

The optimized sample, designated AC5-800, demonstrated exceptional textural properties, achieving a specific surface area of 917.69 m^2/g, along with a micropore volume of 0.487 cm^3/g and a mesopore volume of 0.5167 cm^3/g. This hierarchical pore structure enabled AC5-800 to effectively adsorb pollutants in both gaseous and liquid phases.

The optimization protocols established in this study, specifically the 1:5 KOH ratio and 800 °C activation was not limited to licorice root residue. This method can be effectively translated to other lignocellulosic biomass types common in regional agriculture, such as cherry pits, cottonseed husks, or walnut shells. The inherent similarity in the cellulose-hemicellulose-lignin framework of these materials suggests that they would follow similar pyrolytic and etching pathways, offering a versatile template for localized waste valorization.

The study also revealed that the optimal KOH-to-carbon ratio was 1:5, which led to a total pore volume exceeding 1 cm^3/g—a critical factor for maximizing adsorption efficiency. Increasing the KOH ratio further (to 1:7) triggered partial pore collapse, resulting in reduced pore volume (0.874 cm^3/g) and poorer adsorption performance. In contrast, reducing the KOH ratio to 1:3 enhanced mesopore formation, resulting in mesopore volume of

0.877 cm^3/g. This mesopore-rich structure created favorable adsorption pathways for larger organic and inorganic pollutants, demonstrating how careful adjustment of activation conditions allows tailoring for specific environmental applications.

Comprehensive morphological and structural analyses confirmed that the optimized activated carbons exhibited well-developed porosity alongside a stable amorphous carbon backbone. SEM imaging highlighted a uniform porous network, while XRD analysis verified the absence of crystalline impurities, confirming the successful conversion of biomass into high-quality amorphous carbon. Furthermore, FTIR spectroscopy detected a diverse array of oxygen-containing functional groups—such as hydroxyl, carboxyl, and carbonyl groups—on the carbon surface. These functional groups enhanced the affinity for polar pollutants, further boosting adsorption performance.

The adsorption capacity of the produced activated carbons was also evaluated using methylene blue as a model contaminant. Among the samples, AC5-800 exhibited the highest MB uptake, attributed to its specific surface area of 31.42 m^2/g and pore volume of 0.0497 cm^3/g. Adsorption data fitted well to the Langmuir isotherm (R^2 = 0.995), indicating that the adsorption mechanism followed monolayer coverage on a homogeneous surface. The optimized AC1-800 and AC5-800 demonstrated remarkable performance in removing organic dyes, making them promising options for wastewater treatment applications.

Overall, this work confirms that licorice root residues, previously considered a low-value byproduct, can be upcycled into high-performance activated carbons for environmental remediation. This work not only promotes the circular utilization of industrial waste but also supports the development of cost-effective adsorbents for air and water purification. Future efforts should explore process scaling, compatibility with other chemical activators, and performance testing under real-world conditions to further expand the applicability of these sustainable adsorbents across different environmental sectors.

Acknowledgements

This research was supported by the budget research project of the Colloid Chemistry and Industrial Ecology Laboratory, Institute of General and Inorganic Chemistry, Academy of Sciences of the Republic of Uzbekistan.

REFERENCES

1. Achaw, O. W. (2012). A study of the porosity of activated carbons using the scanning electron microscope. *Scanning Electron Microscopy.* https://doi.org/10.5772/36337
2. Adizov, B. Z., Mukhtor, J. M., Aziz, F., Khujakulov, A., Saloydinov, A., Adizova, N. Z., Begjanova, G. B. (2025). Preparation of anti-detonation additives based on ethanol, oxygen and nitrogen compounds and research of their influence on automobile gasoline. *Processes of Petrochemistry and Oil Refining, 26*(3), 832–841. https://doi.org/10.62972/1726-4685.2025.3.832
3. Ali, I., Asim, M., Khan, T. A. (2012). Low cost adsorbents for the removal of organic pollutants from wastewater. *Journal of Environmental Management, 113*, 170–183. https://doi.org/10.1016/j.jenvman.2012.08.028
4. Askarova, D., Khoshimov, S., Paygamov, R., Abdikamalova, A., Eshmetov, I. (2025). Advancing carbon adsorbents from biomass: Physicochemical analysis of licorice root waste. *AIP Conference Proceedings, 3304*(1), 040011. https://doi.org/10.1063/5.0269548
5. Blachnio, M., Derylo-Marczewska, A., Charmas, B., Zienkiewicz-Strzalka, M., Bogatyrov, V., Galaburda, M. (2020). Activated carbon from agricultural wastes for adsorption of organic pollutants. *Molecules, 25*(21), 5105. https://doi.org/10.3390/molecules25215105
6. Choi, S. W., Lee, C. G. (2015). Adsorption characteristics of functionalized activated carbon for high temperature CO_2 capture. *Journal of the Korean Society of Environmental Engineers, 37*(3), 175–181. https://doi.org/10.4491/KSEE.2015.37.3.175
7. De Gisi, S., Lofrano, G., Grassi, M., Notarnicola, M. (2016). Characteristics and adsorption capacities of low-cost sorbents for wastewater treatment: A review. *Sustainable Materials and Technologies, 9*, 10–40. https://doi.org/10.1016/j.susmat.2016.06.002
8. El Qada, E. N., Allen, S. J., Walker, G. M. (2008). Influence of preparation conditions on the characteristics of activated carbons produced in laboratory and pilot scale systems. *Chemical Engineering Journal, 142*(1), 1–13. https://doi.org/10.1016/j.cej.2007.11.008
9. Garg, R., Garg, R., Sillanpää, M., Alimuddin, Khan, M. A., Mubarak, N. M., et al. (2023). Rapid adsorptive removal of chromium from wastewater using walnut-derived biosorbents. *Scientific Reports, 13*(1), 6859. https://doi.org/10.1038/s41598-023-33843-3
10. Ghorbani, F., Kamari, S., Zamani, S., Akbari, S., Salehi, M. (2020). Optimization and modeling of aqueous Cr (VI) adsorption onto activated carbon prepared from sugar beet bagasse agricultural waste

by application of response surface methodology. *Surfaces and Interfaces, 18*, 100444. https://doi.org/10.1016/j.surfin.2020.100444

11. Harimisa, G., Jusoh, N. W. C., Tan, L., Shameli, K., Ghafar, N. A., Masudi, A. (2022). Synthesis of potassium hydroxide-treated activated carbon via one-step activation method. *Journal of Physics: Conference Series, 2259*, 012009. https://doi.org/10.1088/1742-6596/2259/1/012009
12. Ibrahim, H. S., Jamil, T. S., Hegazy, E. Z. (2010). Application of zeolite prepared from Egyptian kaolin for the removal of heavy metals: II. Isotherm models. *Journal of Hazardous Materials, 182*(1–3), 842–847. https://doi.org/10.1016/j.jhazmat.2010.06.118
13. Jumanazarova, Z. K., Kadirova, Sh. A., Kattaev, N. T., Zakirova, R. P., Muratov, M. M. (2025). New magnesium coordination compound as a "green" plant growth stimulator. *Processes of Petrochemistry and Oil Refining, 26*(2), 574–579. https://doi.org/10.62972/1726-4685.2025.2.574
14. Kalbaev, A., Abdikamalova, A., Asqarova, D., Khoshimov, S., Paygamov, R., Bakhronov, K., Kholikov, K., Salikhanova, D., Jumaeva, D., Eshmetov, I., Maratov, N., Nozim, M. (2026). A study of the structural features and textural properties of carbon sorbents derived from recycled polyethylene terephthalate and polyethylene waste. *Journal of the Mexican Chemical Society*, e2438. https://doi.org/10.29356/jmcs.v70i1.2438
15. Khurmamatov, A. M., Yusupova, N. K., Alimov, N. P., Berdimbetov, S. B., Khametov, Z. M. (2024). Method for increasing the volume of hydrocarbon raw materials through waste processing. *Doklady Chemistry, 515*(1–2), 63–69. https://doi.org/10.1134/S0012500824600627
16. Liu, C., Zhang, H. X. (2022). Modified-biochar adsorbents (MBAs) for heavy-metal ions adsorption: A critical review. *Journal of Environmental Chemical Engineering, 10*(3), 107393. https://doi.org/10.1016/j.jece.2022.107393
17. Liyanaarachchi, H., Thambiliyagodage, C., Lokuge, H., Vigneswaran, S. (2023). Kinetics and thermodynamics study of methylene blue adsorption to sucrose- and urea-derived nitrogen-enriched, hierarchically porous carbon activated by KOH and H_3PO_4. *ACS Omega, 8*(18). https://doi.org/10.1021/acsomega.3c00339
18. Lua, A. C., Yang, T. (2004). Effect of activation temperature on the textural and chemical properties of potassium hydroxide activated carbon prepared from pistachio-nut shell. *Journal of Colloid and Interface Science, 274*(2), 594–601. https://doi.org/10.1016/j.jcis.2003.10.001
19. Luo, Y., Wang, K., Fei, L. (2020). The effects of activation conditions on physical properties of activated carbon. *BioResources, 15*, 7640–7647. https://doi.org/10.15376/biores.15.4.7640-7647
20. Muratov, M., Kurniawan, T. A., Eshmetov, R., Salikhanova, D., Eshmetov, I., Adizov, B., Onn, W. (2024). Promoting sustainability: Micellization and surface dynamics of recycled monoethanolamine surfactants. *Journal of Molecular Liquids, 414*, 126010. https://doi.org/10.1016/j.molliq.2024.126010
21. Muratov, M., Abdikamalova, A., Eshmetov, I., Mamataliyev, N., Xudoyberdiyev, N., Raximov, U., Ergashev, O., Seitnazarova, O., Mamajonov, B. (2025). Waste-derived activated carbons from phenol-formaldehyde and polystyrene: The role of PAN and alkali treatment. *Chemical Review and Letters, 8*(5), 981–1002. https://doi.org/10.22034/crl.2025.532995.1651
22. Muratov, M. M., Abdikamalova, A. B., Seytnazarova, O. M., Najimova, N. B., Salikhanova, D. S., Eshmetov, I. D., Khaydarov, D. M., Abdiraximov, A. X., Paygamov, R. A., Mamataliev, N. N. (2026). Acid-base activation of thermal power plant ash sludge and its adsorption properties towards heavy metals. *Processes of Petrochemistry and Oil Refining, 27*(1), 252–271. https://doi.org/10.62972/1726-4685.2026.1.252
23. Muttil, N., Jagadeesan, S., Chanda, A., Duke, M., Singh, S. K. (2022). Production, types, and applications of activated carbon derived from waste tyres: An overview. *Applied Sciences, 13*(1), 257. https://doi.org/10.3390/app13010257
24. Paryanto, Wibowo, W. A., Hantoko, D., Saputro, M. E. (2019). Preparation of activated carbon from mangrove waste by KOH chemical activation. *IOP Conference Series: Materials Science and Engineering, 543*, 012087. https://doi.org/10.1088/1757-899x/543/1/012087
25. Qu, J., Song, T., Liang, J., Bai, X., Li, Y., Wei, Y., et al. (2019). Adsorption of lead (II) from aqueous solution by modified Auricularia matrix waste: A fixed-bed column study. *Ecotoxicology and Environmental Safety, 169*, 722–729. https://doi.org/10.1016/j.ecoenv.2018.11.085
26. Rakhimov, B., Begzhanova, G., Adizov, B., Bayraeva, N., Jalilov, T., Tanatarov, O., Rajapbaev, X., Temirov, G., Muratov, M. (2025). Evaluation of the physical properties of road bitumen modified with sulfur and high-density polyethylene. *Processes of Petrochemistry and Oil Refining, 26*(3), 999–1008. https://doi.org/10.62972/1726-4685.2025.3.999
27. Ramamoorthy, M., Ragupathy, S., Sakthi, D., Arun, V., Kannadasan, N. (2020). Synthesis of SnO2 loaded on corn cob activated carbon for enhancing the photodegradation of methylene blue under sunlight irradiation. *Journal of Environmental Chemical Engineering, 8*, 104331. https://doi.org/10.1016/j.jece.2020.104331
28. Rizkiana, J., Guan, G., Widayatno, W. B., Hao, X., Li, X., Huang, W., et al. (2014). Promoting effect

of various biomass ashes on the steam gasification of low-rank carbon. *Applied Energy, 133*, 282–288. https://doi.org/10.1016/j.apenergy.2014.07.091

29. Sen, T. K. (2017). Air, gas, and water pollution control using industrial and agricultural solid wastes adsorbents. *CRC Press*. https://doi.org/10.1201/9781351228145
30. Sen, T. K. (2023). Agricultural solid wastes based adsorbent materials in the remediation of heavy metal ions from water and wastewater by adsorption: A review. *Molecules, 28*(14), 5575. https://doi.org/10.3390/molecules28145575
31. Shafeeyan, M. S., Daud, W. M. W. A., Houshmand, A., Shamiri, A. (2010). A review on surface modification of activated carbon for carbon dioxide adsorption. *Journal of Analytical and Applied Pyrolysis, 89*(2), 143–151. https://doi.org/10.1016/j.jaap.2010.07.006
32. Soffian, M. S., Abdul Halim, F. Z., Aziz, F., Rahman, M. A., Mohamed Amin, M. A., Awang Chee, D. N. (2022). Carbon-based material derived from biomass waste for wastewater treatment. *Environmental Advances, 9*, 100259. https://doi.org/10.1016/j.envadv.2022.100259
33. Tibor, S. T., Grande, C. A. (2022). Industrial production of activated carbon using circular bioeconomy principles: Case study from a Romanian company. *Cleaner Engineering and Technology, 7*, 100443. https://doi.org/10.1016/j.clet.2022.100443
34. Usmanov, R., Shakhnoza, K., Sharipova, A., Abdikamalova, A., Eshmetov, R., Eshmetov, I. (2020). Obtaining carbon adsorbents based on local wood waste, research of their physico-chemical and adsorption properties. *Journal of Critical Reviews, 7*(12). https://doi.org/10.31838/jcr.07.12.21
35. Wan Ibrahim, W. M. H., Mohamad Amini, M. H., Sulaiman, N. S., Kadir, W. R. A. (2019). Powdered activated carbon prepared from *Leucaena leucocephala* biomass for cadmium removal in water purification process. *Arabian Journal of Basic and Applied Sciences, 26*(1), 30–40. https://doi.org/10.1080/25765299.2018.1533203
36. Wang, B., Lan, J., Bo, C., Gong, B., Ou, J. (2023). Adsorption of heavy metal onto biomass-derived activated carbon: Review. *RSC Advances, 13*(7), 4275–4302. https://doi.org/10.1039/D2RA07911A
37. Wijewardhana, G. D., Madugalla, T. B., Mantilaka, M. M., Wijesinghe, W., Gunathilake, W. S. (2026). Exploring coconut shell-derived activated carbon black as a green alternative for toner colourants. *RSC Advances, 16*, 6507–6520. https://doi.org/10.1039/D5RA08767H
38. Wu, D., Zhang, W. (2019). Evolution mechanism of macromolecular structure in coal during heat treatment: Based on FTIR and XRD in situ analysis techniques. *Journal of Spectroscopy*, 1–18. https://doi.org/10.1155/2019/5037836
39. Yahya, M. A., Al-Qodah, Z., Ngah, C. W. Z. (2015). Agricultural bio-waste materials as potential sustainable precursors used for activated carbon production: A review. *Renewable and Sustainable Energy Reviews, 46*, 218–235. https://doi.org/10.1016/j.rser.2015.02.051
40. Zhang, H., Guo, X., Zhu, Z. (2017). Effect of temperature on gasification performance and sodium transformation of Zhundong carbon. *Fuel, 189*, 301–311. https://doi.org/10.1016/j.fuel.2016.10.097